Stratiform and Convective Classification of Rainfall Using SSM/I 85-GHz Brightness Temperature Observations

EMMANOUIL N. ANAGNOSTOU

Department of Civil and Environmental Engineering and Iowa Institute of Hydraulic Research, University of Iowa, Iowa City, Iowa

CHRISTIAN KUMMEROW

Mesoscale Atmospheric Processes Branch, Goddard Space Flight Center, National Aeronautics and Space Administration, Greenbelt, Maryland

22 August 1996 and 4 October 1996

ABSTRACT

A better understanding of global climate calls for more accurate estimates of liquid and ice water content profiles of precipitating clouds and their associated latent heating profiles. Convective and stratiform precipitation regimes have different latent heating and therefore impact the earth's climate differently. Classification of clouds over oceans has traditionally been part of more general rainfall retrieval schemes. These schemes are based on individual or combined visible and infrared, and microwave satellite observations. However, none of these schemes report validations of their cloud classification with independent ground observations. The objective of this study is to develop a scheme to classify convective and stratiform precipitating clouds using satellite brightness temperature observations. The proposed scheme probabilistically relates a quantity called variability index (VI) to the stratiform fractional precipitation coverage over the satellite field of view (FOV). The VI for a satellite pixel is the mean absolute 85-GHz brightness temperature difference between the pixel and the eight surrounding neighbor pixels. The classification scheme has been applied to four different rainfall regimes. All four regimes show that the frequency of stratiform rainfall in the satellite FOV increases as the satellite-based VI decreases. The results of this study demonstrate that the satellite-based VI is consistently related to the probability of occurrence of three classes (0%–40%, 40%–70%, and 70%–100%) of FOV stratiform coverage.

1. Introduction

Clouds and precipitation, particularly in the world's tropical regions, play a key role in driving the atmospheric circulation. Roughly three-fourths of the energy absorbed by the earth's atmosphere is derived from the latent heating that results from condensation of water vapor to form precipitation. Two-thirds of this precipitation falls in the tropical regions. Precipitation also impacts the earth's radiation fluxes (e.g., Mitchell et al. 1989), the freshwater flux, and the sea surface temperature (Webster and Lukas 1992).

Most tropical precipitation can be characterized by convective and stratiform systems (Houze 1993). Convective systems are associated with strong vertical velocity fields, small area coverage cells, and high rainfall intensities. Stratiform systems are characterized by widespread slow ascent velocity fields, associated with low rainfall intensities. As a result of the above differences, each system impacts on the ocean mixed layer characteristics and the sea surface temperature differently (Webster and Lukas 1992). Perhaps of even greater importance is the difference in the thermodynamic structure of convective and stratiform systems. Houze (1993) provides an extended discussion on both systems' thermodynamic structure using actual observations and cloud model simulations. Due to the above difference the two systems have different latent heating profiles which impact the earth's climate differently. At low altitudes convective systems heat the atmosphere due to condensation of water vapor, while stratiform systems cool the atmosphere due to evaporation of raindrops. For more details on the convective and stratiform heating profiles and their importance on climate studies the interested reader is referred to Tao et al. (1993a,b), and Simpson et al. (1988). From the remote sensing of rainfall perspective, the convective–stratiform separation may play an important role due to the differences in the inhomogeneity of rainfall within satellite fields of view (FOVs). Inhomogeneity affects retrieval algorithms through what is usually referred to as the ''beamfilling'' corrections. This has been discussed by McConnell and North (1987), Shin and North (1988), Chiu et al. (1988),

Corresponding author address: Emmanouil N. Anagnostou, Institute of Hydraulic Research, University of Iowa, 404 Hydraulic Laboratory, Iowa City, IA 52242-1585.
E-mail: eocnagnos@iihr.uiowa.edu

Bell et al. (1990), and Short and North (1990), among others. Due to the nonlinear nature of the brightness temperature rainfall-rate relations, algorithms that do not consider inhomogeneity would tend to severely underestimate the highly variable convective rainfall. To account for this effect, most credible algorithms employ procedures (either implicitly or explicitly) to correct for the mean beamfilling effect. Unless they explicitly account for the differences in the mean inhomogeneity differences between convective and stratiform precipitation, however, one might expect algorithms to overestimate the relatively homogeneous stratiform precipitation while underestimating the convective component.

Previous satellite-based classification schemes include: 1) combination of infrared and visible channels to classify cloud types (i.e., Shenk et al. 1976; Reynolds and Vonder Haar 1977; Inoue 1987; Rossow and Schiffer 1991), 2) cloud liquid water path based on microwave channels (i.e., Alishouse et al. 1990; Petty 1990; Liu and Curry 1992, 1993; Greenwald et al. 1993), and 3) a latest study by Liu et al. (1995), which combines infrared and microwave satellite data. The cloud classification schemes which are based on visible–infrared combination empirically relate cloud thickness and cloud top with visible and infrared satellite channel data, respectively. However, due to saturation of both channels' radiation very near the cloud top there is no physical relationship between the deep cloud properties and the infrared–visible radiation observables. Cloud classifications which use microwave or combined infrared–microwave data are all part of a more general rainfall retrieval scheme. Although all of these studies have validated their retrieved rainfall with independent ground ''truth'' measurements, none of them has ever reported validations of their classification estimates.

Unlike previous techniques that focus on the radiance information from a single pixel, this study seeks to classify rainfall based upon the spatial variability of rainfall. Convective precipitation regimes are associated with high instabilities and strong updrafts and downdrafts, which result in significant turbulence in the clouds. This turbulence significantly contributes to the variability of both liquid and ice water contents and rainfall rate at the ground. Stratiform precipitation, on the other hand, is characterized by much lower vertical velocities. Variability in liquid and ice water contents as well as surface rainfall is therefore generally much smaller. Based upon this expectation, a variability index (VI) is introduced. For a satellite pixel, the VI is defined by

$$\mathrm{VI} = \frac{1}{N}\sum_{i=1}^{N} |X_i - X_o|, \tag{1}$$

where X_o is the value of the central pixel, X_i are the values of the surrounding pixels, and N is the total number of surrounding pixels used. The value X can be any observed quantity related to rainfall (i.e., satellite brightness temperature).

Contents of the sections are as follows. Section 2 describes the satellite and radar data and procedures used in rainfall classification. Section 3 shows applications of the VI to four radar rainfall regimes, and section 4 presents the classification scheme. Conclusions and recommendations for further research are given in section 5.

2. Data

Special Sensor Microwave/Imager (SSM/I) microwave data have been available continuously since 1987. The sensor consists of four frequencies at 19.35, 22.235, 37.0, and 85.5 GHz. All frequencies except the water vapor absorption channel at 22.235 GHz are dual polarized. The resolution (diffraction limited) of the frequencies ranges from approximately 50 km at 19 GHz to 15 km at 85.5 GHz. The 19-GHz channel responses are dominated by emission processes and therefore respond primarily to increases in the liquid water column over oceans. Over high emissivity land backgrounds, the 19-GHz channels provide little information. The 85-GHz channel, on the other hand, responds primarily to ice-phase hydrometeors. It saturates very quickly with liquid water in the column and then tends to decrease as ice concentrations increase with increasing storm intensities.

Although the 19-GHz channel is physically related to rainfall on the ground, its very low resolution prevents us from using it to classify precipitation. Also, if we assume that high variability of rainfall on the ground is related to high variability of ice content and vice versa, then the 85-GHz channel may be expected to have the ability to measure this variability and identify the precipitation type. Based on the above discussion, it was decided to use the 85-GHz channel of the SSM/I to compute the satellite based variability index. The horizontal polarization ($T_{85\mathrm{H}}$) was chosen because of the early failure of the vertical channel on the *F8* satellite.

Rainfall classification using radar data has been proposed by Steiner et al. (1995). Their classification technique uses the relative pickedness of the horizontal radar reflectivity patterns projected in 2 km $\times$ 2 km rectangular grid, and the reflectivity itself, to predict the echo type (convective/stratiform). The pickedness is defined as the difference between the reflectivity in the classified grid point and the average of the nonzero reflectivities from the neighbor grid points within an 11-km radius. The classification technique has been verified against vertical reflectivity profiles derived from radar data. For further information on the radar-based classification technique, the reader is referred to Steiner et al. (1995).

Figures 1a,b qualitatively illustrate comparisons between corresponding $T_{85\mathrm{H}}$–VI (upper panels) and radar classification (lower panels) maps. Figures 1a and 1b represent two different rainfall regimes: isolated convection (Fig. 1a) and widespread stratiform precipitation (Fig. 1b). Figures 1a,b show that in the vicinity of strong

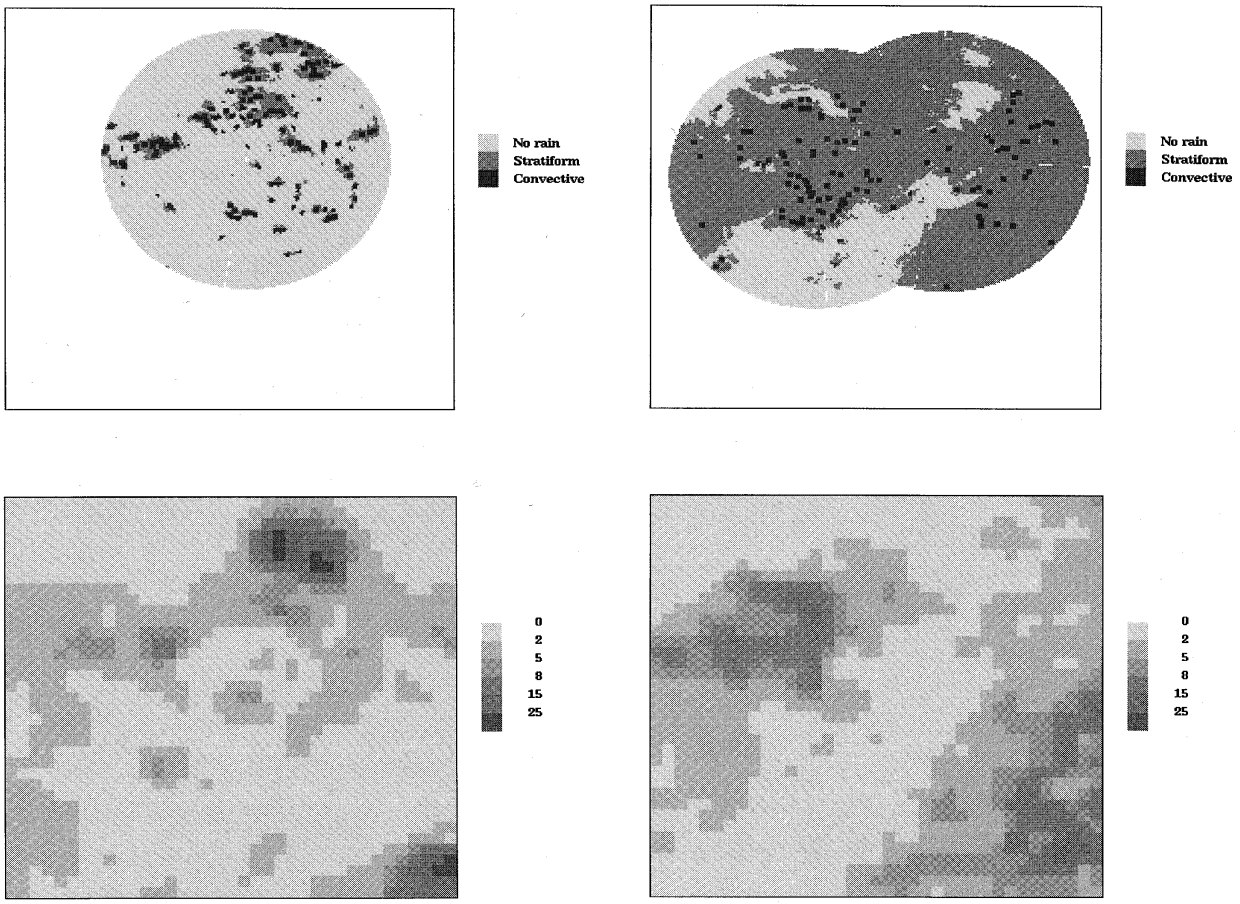

FIG. 1. (a) An example of corresponding radar classification maps and 85-GHz brightness temperature–based VI maps from the TOGA COARE area: (a) left panels, 1858 UTC 19 December 1992; (b) right panels, 1907 UTC 11 February 1993. Radar and satellite maps' resolutions are 4 km^2 and 144 km^2, respectively. The horizontal axis is from 0.54° to 4.55°S in latitude, and the vertical axis is from 153.54° to 157.55°E in longitude.

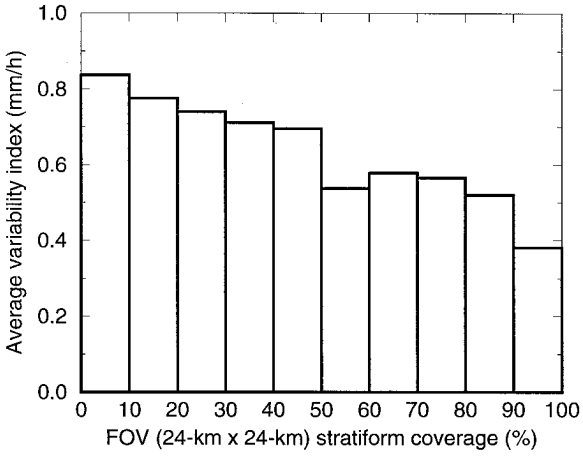

FIG. 2. Average radar rainfall-based variability index versus stratiform fractional coverage.

convection the T_{85H}-based variability index is high. However, the variability index shows a weakness in identifying small intensity and area convective cells. For example, in Fig. 2a the convective cells in southeastern area of radar map do not show any distinct increase of VI values in the corresponding area of VI map. This is a problem associated with satellite spatial sampling limitations.

3. FOV variability index versus stratiform coverage

Figures 1a,b qualitatively illustrate the relationship between T_{85H}-based variability index and the precipitation type. The purpose of this study, however, is to develop quantitative relationships that can be used in subsequent studies. It was decided that satellite navigation errors and FOV spatial sampling limitations would make any deterministic relationship very difficult to establish. Probabilistic relationships, on the other hand, can practically deal with the uncertainty introduced by the above problems.

TABLE 1. Rainfall regimes' locations and time periods.

Location	Latitude	Longitude	Time period
TOGA COARE 1	0°–5°S	153°–158°E	10 Dec 92–20 Jan 93
TOGA COARE 2	0°–5°S	153°–158°E	20 Jan 93–28 Feb 93
Darwin, Australia	11°–14°S	129.5°–132.5°E	24 Dec 93–30 Jan 94
Melbourne, Florida	0°–5°S	79.0°–82.2°W	1 Jul 93–31 Aug 93

The concept of probabilistically relating the variability index to the convective/stratiform fractional coverage of rainfall areas is first tested using the Tropical Oceans Global Atmosphere Coupled Ocean–Atmosphere Response Experiment (TOGA COARE) radar rainfall data. First, the variability index [Eq. (1)] corresponding to each 2-km radar rainfall pixel is computed. This variability index is then averaged to 24-km resolution chosen to correspond roughly to current and future sensor resolutions. Finally, the conditional (rainfall rate greater than 0.1 mm h^{-1}) stratiform fractional coverage of the large areas is computed from the radar based convective/stratiform classification maps. Figure 2 displays the average VI versus the percentage of stratiform coverage over the large area. It is clear that as stratiform coverage increases the average VI decreases. This observation supports the assertion made in the previous section that ''beam-filling'' problems are likely to affect convective and stratiform precipitation differently. It also raises hopes that variability index as defined in Eq. (1) is a good indicator of stratiform–convective precipitation type. However, it still remains to be shown how the VI computed from the spaceborne observations can relate to precipitation type.

Four different radar rainfall regimes have been chosen to identify the probabilistic relationship between satellite field of view VI and stratiform coverage. Table 1 shows the rainfall regimes' locations (latitude–longitude) and time periods. The first two rainfall regimes, although belonging to the same geographic location (TOGA COARE area), represent two different precipitation systems. The first typical synoptic condition was dominated by stratiform precipitation, quite unusual for tropical oceanic precipitation, while the second was mainly convective cells with less stratiform precipitation areas. The third rainfall regime at Darwin, Australia, mainly consists of squall-line convective systems trailed by large stratiform areas. Isolated convective cells and imbedded convection within small stratiform areas characterize the fourth rainfall regime at Melbourne, Florida. Darwin and Melbourne are two of the ground validation radar sites of NASA's Tropical Rainfall Measuring Mission (Simpson et al. 1988).

TABLE 2. Analysis of the corresponding radar–satellite data.

Location	Over-passes	Total points	Wet points
TOGA COARE 1	87	127 387	4264
TOGA COARE 2	77	113 394	2530
Darwin, Australia	120	59 403	8724
Melbourne, Florida	157	78 791	3277

The identification of the satellite FOV VI–stratiform coverage relationship was based on the corresponding radar–satellite matched points from the above rainfall regimes. Table 2 gives the number of satellite overpasses, total radar–satellite matched points, and rainy radar–satellite matched points, for each rainfall regime. The radar–satellite matched points were generated by finding the corresponding radar pixels within a 6-km radius from every 85-GHz satellite FOV position (latitude/longitude). The radar maps are in Cartesian coordinates with 2 km $\times$ 2 km pixel resolution. Radar data were used to estimate the satellite FOV area ground ''true'' rainfall type (convective/stratiform) and volume. Ciach et al. (1997) and Steiner et al. (1995) provide a detailed discussion on the algorithms that were used to retrieve rainfall-rate and classification maps from volume scan radar reflectivities.

Figure 3 illustrates the relationship between satellite FOV variability index and stratiform coverage. Figures 3a–d correspond to the first, second, third, and fourth rainfall regimes respectively. The FOV area is approximately 12 km $\times$ 12 km. The horizontal axis corresponds to the T_{85H}-based VI and is divided into seven classes (0–4, 4–8, 8–16, 16–20, 20–24, and 24–28). Within each VI class the fraction of satellite FOV total rain volume (normalized frequency) of three stratiform coverages (0%–40%, 40%–70%, and 70%–100%) is plotted. Stratiform coverage is defined as the ratio of the satellite FOV stratiform versus total (convective plus stratiform) precipitation area. The normalized frequency of a variable can be statistically interpreted as probability of occurrence of this variable—this is the term we will be using from now on. It is very interesting to notice that all four rainfall regimes show similar results. Namely, at small VI values the probability of occurrence of satellite FOV areas with large stratiform coverage ($> 70\%$) is high (≥ 0.6). It is also common for all three rainfall regimes that increasing the VI value the probability of occurrence of high ($> 70\%$) and low ($< 40\%$) stratiform coverages decrease and increase, respectively. The strong agreement between the results of all four rainfall regimes is an indicator of a universal relationship between satellite FOV VI and stratiform coverage.

4. Classification scheme

The results of Fig. 3 provide the conceptual basis of the classification scheme. The scheme first computes the

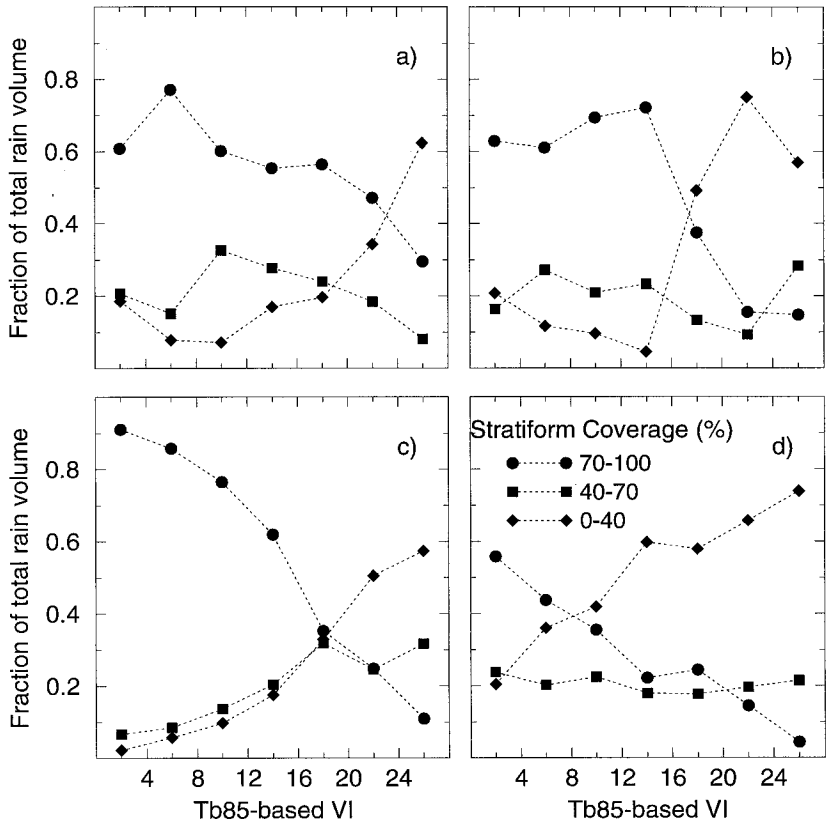

FIG. 3. Probability of occurrence of three discrete ranges of satellite FOV fractional stratiform coverage vs 85-GHz brightness temperature–based VI. Panels (a)–(d) correspond to the first, second, third, and fourth rainfall regimes, respectively.

VI values from the satellite 85-GHz horizontal polarization brightness temperature T_{85H} observations. Next, it uses the computed VI values to provide the probability of occurrence of three satellite FOV percentages of stratiform coverage (0%–40%, 40%–70%, and 70%–100%). The probabilistic relationship between the stratiform coverage over the satellite FOV and the T_{85H}-based VI, based on Fig. 3, is shown in Table 3.

5. Conclusions and future research

A probabilistically based convective–stratiform classification scheme has been developed. The scheme relates a quantity called variability index, computed from 85-GHz brightness temperature observations, to the precipitation type. Due to errors discussed in section 3, the relationship is defined in a probabilistic framework. Namely, given the computed VI from the 85-GHz brightness temperatures the scheme provides the probability of high (> 70%), moderate (40%–70%), and low (< 40%) percentages of stratiform coverage over the satellite FOV rainfall area. Figure 3 showed that this information can be reliably provided from the variability index. Low variability index is related to high probability of large fractional stratiform coverage and vice versa.

This study has focused primarily upon tropical rainfall regimes using case studies from the western Pacific—Darwin and Melbourne. Datasets currently being developed for standard products in connection with the Tropical Rainfall Measuring Mission will be analyzed in the future to verify consistency with the current results. Efforts will also be made to acquire extratropical datasets in order to assess the convective–stratiform differences in those regimes. In the future, we intend to both validate the findings of this study with other rainfall regimes and apply the results from this study for improved quantification of rainfall rates and types through rainfall retrieval algorithms such as the Goddard profiling algorithm (C. Kummerow et al. 1997, manuscript submitted to *J. Appl. Meteor.*).

TABLE 3. Classification scheme—probability of occurrence of stratiform coverage for three ranges of VI values.

	Stratiform coverage (%)		
	>70%	40%–70%	<40%
VI	Probability of occurrence—mean (range)		
0–8	0.67 (0.45–0.91)	0.17 (0.07–0.27)	0.15 (0.02–0.20)
8–24	0.44 (0.15–0.75)	0.21 (0.10–0.33)	0.34 (0.09–0.65)
>24	0.15 (0.05–0.30)	0.22 (0.08–0.30)	0.63 (0.57–0.62)

Acknowledgments. The authors would like to thank Mr. Louis Giglio for helping them process the SSM/I data and Dr. Bill Olson for his valuable discussions. We would also like to thank the two anonymous reviewers for their comments. The work was carried out at the Mesoscale Atmospheric Processes Branch of Goddard Space Flight Center (GSFC), NASA, where Mr. Emmanouil N. Anagnostou was a 1995 USRA/GSFC Graduate Student Summer Program participant.

REFERENCES

Alishouse, J. C., J. B. Snider, E. R. Westwater, C. T. Swift, C. S. Ruf, S. A. Snyder, J. Vongsathorn, and R. R. Ferraro, 1990: Determination of cloud liquid water content using SSM/I. *IEEE Trans. Geosci. Remote Sens.,* **28,** 817–822.

Bell, T. L., A. Abdullah, L. M. Russell, and G. R. North, 1990: Sampling errors for satellite-derived tropical rainfall: Monte Carlo study using a space–time stochastic model. *J. Geophys. Res.,* **95,** 2195–2205.

Chiu, L. S., G. R. North, and D. A. Short, 1988: Errors in satellite rainfall estimation due to nonuniform field of view of spaceborne microwave sensors. *Proc. IUGG Conf. on Microwave Remote Sensing,* Hampton, VA, Int. Union Geodesy Geophys.

Ciach, G. J., W. F. Krajewski, E. N. Anagnostou, M. L. Baeck, J. R. McCollum, A. Kruger, and J. A. Smith, 1997: Radar rainfall estimation for ground validation studies of the tropical rainfall measuring mission. *J. Appl. Meteor.,* **36,** 735–747.

Greenwald, T. J., G. L. Stephens, T. H. Vonder Haar, and D. L. Jackson, 1993: A physical retrieval of cloud liquid water over the global oceans using Special Sensor Microwave/Imager (SSM/I) observations. *J. Geophys. Res.,* **98,** 18 471–18 488.

Houze, R. A., 1993: *Cloud Dynamics.* Academic Press, 573 pp.

Inoue, T., 1987: A cloud type classification with NOAA 7 split-window measurements. *J. Geophys. Res.,* **92,** 3991–4000.

Liu, G., and J. A. Curry, 1992: Retrieval of precipitation from satellite microwave measurement using both emission and scattering. *J. Geophys. Res.,* **97,** 9959–9974.

——, and ——, 1993: Determination of characteristic features of cloud liquid water from satellite microwave measurements. *J. Geophys. Res.,* **98,** 5069–5092.

——, ——, and R.-S. Sheu, 1995: Classification of clouds over the western equatorial Pacific Ocean using combined infrared and microwave satellite data. *J. Geophys. Res.,* **100,** 13 811–13 826.

McConnell, A., and G. R. North, 1987: Sampling errors in satellite estimates of tropical rain. *J. Geophys. Res.,* **92,** 9567–9570.

Mitchell, J. F. B., C. A. Senior, and W. J. Ingram, 1989: $C0_2$ and climate: A missing feedback? *Nature,* **341,** 132–134.

Petty, G. W., 1990: On the response of the Special Sensor Microwave/Imager to marine environment—Implications for atmospheric parameter retrievals. Ph.D. dissertation, University of Washington, 291 pp.

Reynolds, D. W., and T. H. Vonder Haar, 1977: A bispectral method for cloud parameter determination. *Mon. Wea. Rev.,* **105,** 446–457.

Rossow, W. B., and R. A. Schiffer, 1991: ISCCP cloud data products. *Bull. Amer. Meteor. Soc.,* **72,** 2–20.

Shenk, W. E., R. J. Holub, and R. A. Neff, 1976: A multispectral cloud type identification method using Nimbus-3 MRIR measurements. *Mon. Wea. Rev.,* **104,** 284–291.

Shin, K.-S., and G. R. North, 1988: Sampling error study for rainfall estimate by satellite using a stochastic model. *J. Appl. Meteor.,* **27,** 1218–1231.

Short, D. A., and G. R. North, 1990: The beam filling error in the Nimbus 5 electronically scanning microwave radiometer observations of Global Atlantic Tropical Experiment rainfall. *J. Geophys. Res.,* **95,** 2187–2193.

Simpson, J., R. F. Adler, and G. R. North, 1988: A proposed Tropical Rainfall Measuring Mission (TRMM) satellite. *Bull. Amer. Meteor. Soc.,* **69,** 278–295.

Steiner, M., R. A. Houze, and S. E. Yuter, 1995: Climatological characterization of three-dimensional storm structure from operational radar and rain gauge data. *J. Appl. Meteor.,* **34,** 1978–2007.

Tao, W.-K., S. Lang, J. Simpson, and R. Adler, 1993a: Retrieval algorithms for estimating the vertical profiles of latent heat release: Their applications for TRMM. *J. Meteor. Soc. Japan,* **71,** 685–700.

——, J. Simpson, C.-H. Sui, S. Lang, J. Scala, B. Ferrier, M.-D. Chou, and K. Pickering, 1993b: Heating, moisture, and water budgets of tropical and midlatitude squall lines: Comparisons and sensitivity to longwave radiation. *J. Atmos. Sci.,* **50,** 673–690.

Webster, P. J., and R. Lukas, 1992: TOGA COARE: The Coupled Ocean–Atmosphere Response Experiment. *Bull. Amer. Meteor. Soc.,* **73,** 1377–1416.